Mo(V) co-ordination in the periplasmic nitrate reductase from *Paracoccus pantotrophus* probed by electron nuclear double resonance (ENDOR) spectroscopy

Clive S. BUTLER*†[1], Shirley A. FAIRHURST‡, Stuart J. FERGUSON§, Andrew J. THOMSON†, Ben C. BERKS*, David J. RICHARDSON† and David J. LOWE‡[2]

*School of Biological Sciences, Centre for Metalloprotein Spectroscopy and Biology, University of East Anglia, Norwich NR4 7TJ, U.K., †School of Chemical Sciences, Centre for Metalloprotein Spectroscopy and Biology, University of East Anglia, Norwich NR4 7TJ, U.K., ‡Biological Chemistry Department, John Innes Centre, Colney Lane, Norwich NR4 7UH, U.K., and §Department of Biochemistry, University of Oxford, Oxford OX1 3QU, U.K.

The first electron nuclear double resonance (ENDOR) study of a member of the Mo-*bis*-molybdopterin guanine dinucleotide family of molybdoenzymes is presented, using the periplasmic nitrate reductase from *Paracoccus pantotrophus*. Rapid freeze-quenched time-resolved EPR revealed that during turnover the intensity of a Mo(V) EPR signal known as High-*g* [resting] increases. This signal is split by two interacting protons that are not solvent-exchangeable. X-band proton-ENDOR analysis resolved broad symmetrical resonance features that arose from four classes of protons weakly coupled to the Mo(V). Signals from two of these were lost upon exchange into deuterated buffer, suggesting that they may originate from OH or H_2O groups. One of these signals was also lost when the enzyme was redox-cycled in the presence of azide. Since these protons are very weakly coupled OH/H_2O groups, they are not likely to be ligated directly to the Mo(V). This suggests that protonation of a Mo(VI)=O group does not occur on reduction to Mo(V), but most probably accompanies reduction of Mo(V) to Mo(IV). A resonance feature from a more strongly coupled proton, that was not lost following exchange into deuterated buffer, could also be resolved at 22–24 MHz. The anisotropy of this feature, determined from ENDOR spectra collected at a range of field positions, indicated a Mo–proton distance of approx. 3.2 Å, consistent with this being one of the β-methylene protons of a Mo–Cys ligand.

Key words: cysteine, EPR, molybdoenzymes, molybdopterin guanine dinucleotide (MGD), protons.

INTRODUCTION

Of the three distinct classes of enzyme that carry out the bacterial reduction of nitrate to nitrite, two are associated with energy-conserving respiratory electron transport pathways and one with nitrate assimilation [1]. One class of respiratory enzymes is membrane-anchored with an active site in the cytoplasm, and the other is water-soluble and periplasmic [2]. The assimilatory enzymes are located in the cytoplasm [1]. Sequence analysis has revealed that all bacterial nitrate reductases are members of the subgroup of molybdoenzymes that bind the molybdopterin guanine dinucleotide (MGD) form of the molybdopterin cofactor [2]. The soluble periplasmic nitrate reductase (NAP_{Pp}) from *Paracoccus pantotrophus* (previously classified as *Paracoccus denitrificans* GB17 and *Thiosphaera pantotropha* [3]) contains a 16 kDa di-haem *c*-type cytochrome subunit (NapB) and a 90 kDa catalytic subunit (NapA) that binds an N-terminal [4Fe–4S] cluster and the MGD [2,4–7]. The catalytic subunit exhibits a high degree of sequence similarity to the MGD-binding polypeptides of bacterial assimilatory nitrate reductases (NASs) and formate dehydrogenases, both of which also bind an N-terminal iron–sulphur cluster and MGD [2,8]. NAP and NAS are quite distinct from the membrane-bound nitrate reductase (NAR), which is a three-subunit enzyme consisting of an integral membrane di-*b*-haem cytochrome, a water-soluble electron-transferring subunit that binds four iron–sulphur clusters, and a large 120–140 kDa catalytic subunit that binds the MGD [2].

The crystal structure of monomeric NAP from *Desulfovibrio desulfuricans* (NAP_{Dd}) has been reported recently, confirming the presence of two MGD moieties per Mo (Mo-*bis*-MGD) [9]. This is consistent with the crystal structures of three other members of the MGD family, namely the soluble periplasmic DMSO reductases from *Rhodobacter capsulatus* and *Rhodobacter sphaeroides*, the soluble formate dehydrogenase H (FdhH) from *Escherichia coli*, and the periplasmic trimethylamine *N*-oxide reductase from *Shewanella massilia* [10–14]. These two MGD moieties can provide up to four thiolate ligands to the Mo, although in the case of one structure of the DMSO reductase the di-thiol of one MGD moiety is not co-ordinated to the Mo [11]. This indicates some flexibility in the catalytic site, and this is reflected in the range of different Mo(V) EPR signals observed for this enzyme [15]. In DMSO reductase the polypeptide chain provides a Ser-O-ligand to the Mo, and there may be one or two oxo-group ligands in the Mo(VI) state. In FdhH a selenocysteine provides a Se ligand to the Mo, and a hydroxo group is additionally present in the Mo(VI) state. The crystal structure of NAP_{Dd} suggests a des-oxo Mo(VI) state with a water/hydroxo ligand and a Cys ligand provided by the polypeptide chain [9]. From this structure, Romão and co-workers [9] proposed that NAP_{Dd} cycles between des-oxo Mo(IV) and mono-oxo Mo(VI), which is then readily protonated to form the water/hydroxo ligand. Such a mechanism is similar to that proposed for FdhH from *E. coli*. This may not be surprising, given that there is a high degree of sequence identity between *E. coli* FdhH and NAP_{Dd}. In fact

Abbreviations used: ENDOR, electron nuclear double resonance; FdhH, formate dehydrogenase H; MGD, molybdopterin guanine dinucleotide; NAP, periplasmic nitrate reductase; NAP_{Dd}, NAP from *Desulfovibrio desulfuricans*; NAP_{Pp}, NAP from *Paracoccus pantotrophus*; NAR, membrane-bound nitrate reductase; NAS, assimilatory nitrate reductase.

[1] Present address: School of Biochemistry and Genetics, The Medical School, University of Newcastle, Newcastle NE2 4HH, U.K.
[2] To whom correspondence should be addressed (e-mail david.lowe@bbsrc.ac.uk).

NAP_{Dd} enzyme also has low formate dehydrogenase activity, and primary structure analysis reveals that it is actually a rather divergent member of the NAP family. NAP_{Pp} does not have formate dehydrogenase activity [16], clearly highlighting catalytic differences between NAPs from these two sources.

Recently, we have reported a detailed study of Mo co-ordination in NAP_{Pp} using EPR and EXAFS spectroscopies [16]. These results suggest distinct molybdenum co-ordination environments in the Mo(VI) and Mo(IV) oxidation states. In the oxidized state, Mo(VI) is co-ordinated by five sulphur and two oxo ligands. Of the sulphur ligands, four are likely to be provided by the two pterins at a distance of 2.43 Å. The fifth sulphur ligand is at a distance of 2.82 Å and, based upon primary structure analysis and site-directed mutagenesis (H. J. Sears, unpublished work), is suggested to be provided by a co-ordinating cysteine residue (Cys^{181}). Upon reduction by dithionite, Mo(IV) becomes tetraco-ordinate by the loss of one oxo and two sulphur ligands. The heptaco-ordinate species is recovered upon re-oxidation by nitrate. This has suggested that the NAP_{Pp} complex can cycle between a Mo(VI) di-oxo species and a Mo(IV) mono-oxo species during a catalytic cycle [16].

While much attention has been given to determining the nature and number of co-ordinating ligands to both Mo(IV) and Mo(VI) species, little structural information has been obtained for the NAP Mo(V) species, which may form an important intermediate during the reductive half of the catalytic cycle. EPR analysis of Mo(V) from NAP_{Pp} has revealed a number of different signals that probably arise from a number of different structural forms [16,17]. The 'as prepared' enzyme displays a Mo(V) EPR signal with a g_{av} of 1.98 that represents approx. 5–10 % of the total molybdenum in the oxidized sample. The Mo(V) EPR spectrum exhibits rhombic symmetry with unusually low anisotropy and is split by two $I = \frac{1}{2}$ nuclei, presumably protons. These weak interactions are still apparent in spectra collected from enzyme exchanged into ^2H_2O, suggesting that they do not arise from the protons of Mo–OH or $Mo–OH_2$ groups. In the present study, this Mo(V) High-*g* [resting] species has been observed during rapid turnover of NAP_{Pp} using rapid-freeze quench EPR techniques, and the signal has been studied using electron nuclear double resonance (ENDOR) spectroscopy to probe the origin of the weakly interacting protons. ENDOR has been widely used to develop catalytic models for molybdenum hydroxylases, e.g. xanthine oxidase [18,19], but the present paper presents the first detailed ENDOR characterization of a *bis*-MGD enzyme.

EXPERIMENTAL

Purification and sample preparation

P. pantotrophus strain M6 was grown under anaerobic denitrifying conditions, and the NapAB complex was purified as described by Berks et al. [5]. Purified samples were routinely prepared in 20 mM Hepes, pH 7.2, and concentrated to $\sim 300\ \mu M$ or $\sim 600\ \mu M$ for EPR and ENDOR analysis respectively. Samples were exchanged into ^2H_2O buffer containing 20 mM Na Hepes, pH* 7.2. pH* is the apparent pH of the buffer in ^2H_2O measured with a standard glass pH electrode.

EPR and ENDOR spectroscopy

EPR spectroscopy was performed on an updated X-band ER200-D spectrometer (Bruker Spectrospin) interfaced to an ESP1600 computer and fitted with a liquid helium flow cryostat (Oxford Instruments ESR-900, modified to take sample tubes of up to 4 mm internal diameter). Mo(V) EPR spectra were generally recorded at 60 K, ~ 9.64 GHz microwave frequency, 2 mW microwave power and 0.1 mT field modulation amplitude at 100 kHz, unless stated otherwise in the text or Figure legends. The spin concentration of samples was determined from integrations of their EPR absorption spectra compared with those of a 2 mM Cu^{II}-EDTA standard, as described in earlier work [20]. For rapid-reaction studies, samples of NapAB complex were pre-reduced with dithionite (2 mM) in the presence of Methyl Viologen (10 μM) in an anaerobic glove box where typical oxygen levels were below 1 p.p.m. The pre-reduced samples were reacted with nitrate (10 mM) on a millisecond time scale using the freeze–quench apparatus described previously [21].

X-band ENDOR spectra were recorded on the same Bruker ER200-SRC spectrometer and cooling system equipped with an ENDOR/triple accessory and a radio-frequency amplifier of 100 W nominal output power (ENI 3100LA). Recording conditions are specified in the Figure legends. Microwave power and temperature were selected for optimum signal/noise. All ENDOR spectra were accumulated over extended periods of up to 48 h, to obtain adequate signal/noise ratios. Field stability is better than 0.01 mT over such time periods once the spectrometer has equilibrated for 4 h.

Analysis of ENDOR spectra

When the hyperfine interaction, A^H, between an unpaired electron and a proton is less than ν_H, the free proton Larmor frequency, which is equal to $g_H\beta_n H_0/h$ (where g_H is the proton *g*-value of 5.59, β_n is the nuclear magneton and h is Planck's constant; $\nu_H = 14.90$ MHz, when the magnetic field $H_0 = 350$ mT), a set of magnetically equivalent protons is expected to give a single pair of ENDOR transitions separated by A^H and mirrored about ν_H at frequencies:

$$\nu\pm(H) = \nu_H \pm A^H/2$$

When $A^H > \nu_H$, the pair is centred on $A^H/2$ and split by $2\nu_H$, such that:

$$\nu\pm(H) = A^H/2 \pm \nu_H$$

Distance information can be obtained from proton ENDOR spectra, since at large distances the principal term contributing to the anisotropy of the hyperfine interaction is the through-space dipolar interaction between the nuclear and electronic spins, although this approach has limitations [22,23], as discussed below. The dipolar interaction has the form:

$$A_D = g_e\beta_e g_H\beta_n(3\cos^2\phi - 1)\rho/hr^3$$

where g_e and β_e are the electronic *g*-factor and Bohr magneton respectively, g_H and β_n are the proton *g*-factor and nuclear magneton respectively, ϕ is the angle between the line joining the spins and the magnetic field direction, r is the distance between the spins, and ρ is the spatial distribution of the electronic spin. A_D therefore has maximum and minimum values when $\phi = 0°$ or 90°, so that $\cos^2\phi = 1$ or 0 and $(3\cos^2\phi - 1)$ is 2 or -1. Thus the total anisotropy is $3g_e\beta_e g_H\beta_n/hr^3$. It is possible to measure this anisotropy from ENDOR spectra acquired at a number of points across the EPR spectrum, covering all possible orientations (ϕ) of the system, and this contains only one unknown, r, the distance between the spins, which is therefore easily calculated. Corrections occur when the orbital containing the unpaired electron includes a significant contribution from a bonding orbital involving the nucleus being considered; under these conditions, local terms can dominate the anisotropic interaction; however, for hydrogen atoms the *2p* orbitals are so inaccessible that this contribution is always essentially zero. The final problem

lies with estimating ρ, the spatial distribution of the unpaired spin, and integrating the dipolar interaction over the singly occupied molecular orbital. A good approximation for contributions from distant atoms is to assume that the electron distribution can be represented as a point charge positioned at the nucleus. However, for closer atoms, it is necessary to perform the integration over the orbitals to obtain accurate values; this is impossible for complex, ill-defined cases such as that considered in the present paper, so that only approximate distances can be obtained.

RESULTS AND DISCUSSION

A Mo(V) EPR signal, termed the High-*g* [resting] signal [16,20], can be detected in the 'as prepared' resting NAP_{Pp} (Figure 1). The intensity of the signal exhibits preparation-to-preparation variability, but always lies in the range of 2.5–10 % of total Mo. It displays rhombic symmetry and exhibits unusually low anisotropy ($g_1 - g_3 = 0.018$). The signal is split by two weakly interacting $I = \frac{1}{2}$ nuclei, $A_1^1 = 17.83$ MHz and $A_1^2 = 7.85$ MHz. The weaker splitting can be resolved in the g_1 region only. Under slow turnover conditions with dithionite as electron donor ($k_{cat} = 1\ s^{-1}$) the features of the High-*g* [resting] EPR signal change slightly to yield the so-called High-*g* [nitrate] signal, which we have suggested previously may have catalytic relevance or be a product-bound dead-end species [16,20]. To investigate which EPR signals are catalytically relevant under more rapid turnover conditions, NAP_{Pp} turnover was studied using Methyl Viologen as a redox mediator. NAP_{Pp} (100 μM) was reduced with dithionite (2 mM) in the presence of Methyl Viologen (10 μM) in an anaerobic glove box. Samples were then reacted with excess nitrate (10 mM) and the reactions were quenched on a time scale of 5–500 ms using the rapid freeze–quench apparatus. EPR analysis at 10 K of the 0 ms (zero substrate concentration) samples confirmed that the two NapB haems and the NapA iron–sulphur centre were reduced. A weak Mo(V) signal that accounted for only 3.8 % of total Mo was also detected at 60 K. Assuming that the remaining molybdenum is in the Mo(IV) state, the NapAB complex carries at least five electrons prior to being exposed to nitrate. The residual Mo(V) EPR signal of the reduced enzyme had the form of the High-*g* signal (Figure 2). Following the reaction with nitrate, the Mo(V) High-*g* [resting] signal increased in intensity until it reached a maximum at ~ 40 ms (12.5 % of the total Mo). The k_{cat} of NAP_{Pp} with dithionite and Methyl Viologen as the electron-donor system is approx. 240 s^{-1} [16]. Consequently, in the rapid freeze–quench reaction, the electron donor (dithionite) will be consumed in approx. 20 ms. This corresponds well with the 13–40 ms time scale over which the maximum Mo(V) signal appears. A longer reaction time (up to 500 ms) did not change the intensity or form of the Mo(V) High-*g* [resting] signal. We are not able to exclude the possibility that this signal arose from a dead-end species generated during turnover of NAP_{Pp}. However, the fact that no other Mo(V) species accumulated transiently during the experimental time course suggests that the High-*g* [resting] species, rather than the High-*g* [nitrate] species identified previously under slow-turnover conditions [16], is an intermediate in the

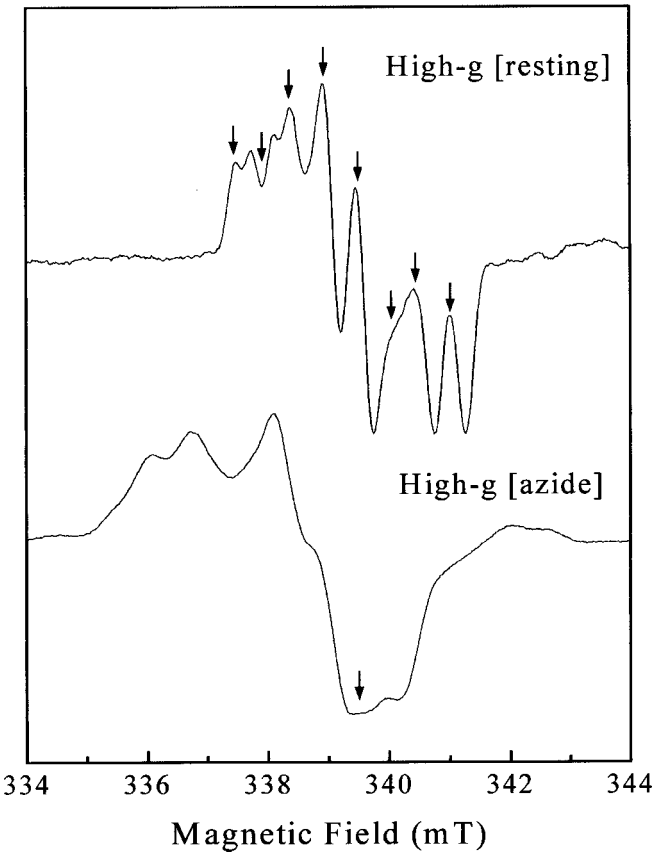

Figure 1 X-band EPR spectrum of Mo(V) High-*g* [resting] and High-*g* [azide] signals of NAP_{Pp}

The enzyme concentration was 277 μM in 20 mM Hepes, pH 7.2. Arrows indicate the field positions where ENDOR spectra were recorded. Conditions of measurement: microwave frequency, 9.64 GHz; microwave power, 2 mW; modulation amplitude, 0.1 mT; temperature, 60 K.

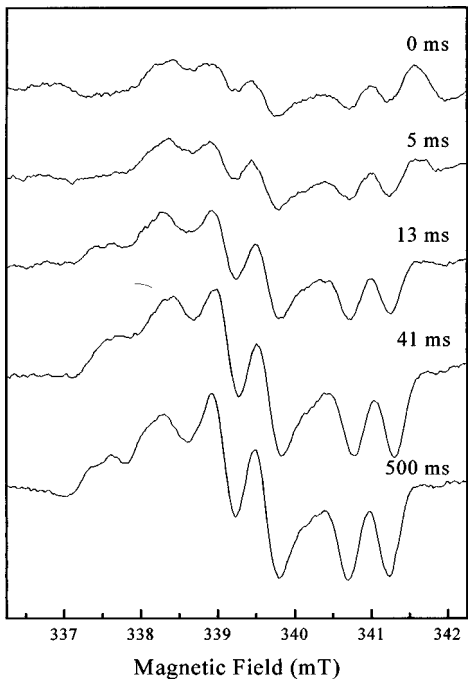

Figure 2 Time course of the development of the Mo(V) High-*g* [resting] signal of NAP_{Pp} when reacted rapidly with excess nitrate

Conditions of measurement: microwave frequency, 9.64 GHz; microwave power, 2 mW; modulation amplitude, 0.1 mT; temperature, 60 K.

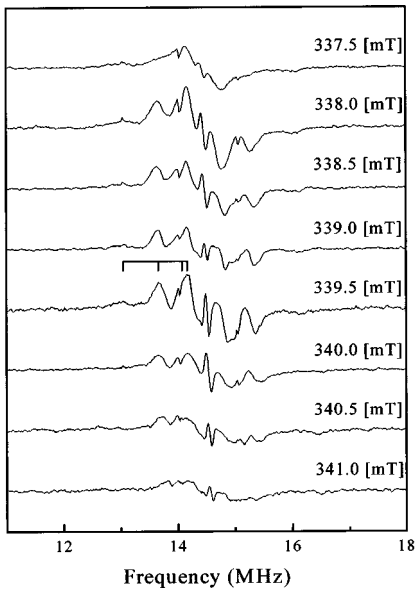

Figure 3 X-band ENDOR spectra (11–18 MHz) of the Mo(V) High-*g* [resting] signal, measured at 25 K

ENDOR fields are indicated. Conditions: frequency, 9.47 GHz; microwave power, 5 mW; (nominal) radio frequency (RF) power, 100 W; RF modulation depth, 100 kHz.

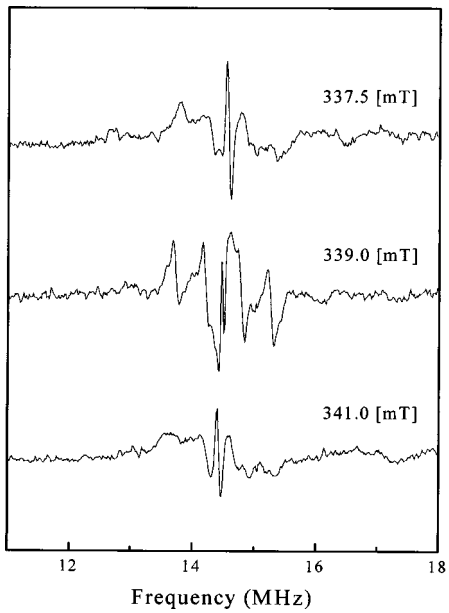

Figure 4 X-band ENDOR spectra (11–18 MHz) of the Mo(V) High-*g* [resting] signal after ^2H_2O exchange, measured at 25 K

ENDOR fields are indicated. Conditions: frequency, 9.47 GHz; microwave power, 5 mW; (nominal) radio frequency (RF) power, 100 W; RF modulation depth, 100 kHz.

catalytic cycle of NAP_{Pp} under Methyl Viologen-mediated rapid-turnover conditions. It is pertinent to note that that this signal has also been detected previously in intact cell suspensions, suggesting a possible physiological relevance [24].

The detection of the High-*g* [resting] signal during rapid turnover led us to study the Mo co-ordination of this species in more detail using ENDOR. Samples of NAP_{Pp} were prepared for ENDOR in H_2O and ^2H_2O. In both cases the presence of the High-*g* [resting] Mo(V) EPR signal, split by the two weakly interacting $I = \frac{1}{2}$ nuclei, was confirmed (Figure 1, shown for H_2O sample only). As discussed above, the detection of these interactions in spectra collected from enzyme exchanged into deuterated buffer suggests that they do not originate from the protons of Mo–OH or Mo–OH_2 ligands [16,20]. High-resolution ^1H ENDOR spectra of NAP_{Pp} (H_2O) were collected at eight field positions across the High-*g* [resting] Mo(V) EPR spectrum (Figure 3; note that sharp features at integer MHz frequencies are spectrometer artifacts). Of these positions, g_x (337.5 mT) and g_z (341.0 mT) represent unique molecular orientations. Visual inspection of the ENDOR spectra confirms that their intensity changes correspondingly with the EPR intensity, and the centre of gravity increases with magnetic field. At g_y (field 339.5 mT), the ^1H ENDOR spectrum clearly displays broad features centred at $\nu_H \sim 14.5$ MHz, with resonances to both low and high frequency of ν_H that arise from coupled protons. There appear to be about four resolved pairs of proton resonances in the 13–16 MHz region arranged symmetrically around ν_H (indicated in Figure 3). ENDOR spectra of NAP_{Pp} exchanged into ^2H_2O buffer were recorded at three field positions across the EPR spectrum, and a number of resonances from weakly interacting protons could again be detected in the 13–16 MHz region (Figure 4). However, comparison of the ENDOR spectra of NAP_{Pp} (H_2O) and NAP_{Pp} (^2H_2O) recorded at 337.5 mT (g_x) clearly show that a weakly coupled proton, with resonance-intense features at 13.8 and 14.8 MHz ($A^H \sim 1.0$ MHz), is lost upon exchange into deuterated buffer (Figure 5). This completely changes the shape of the ENDOR spectrum around ν_H. In addition, a more strongly coupled proton giving rise to weak resonances at 13 and 16 MHz ($A^H \sim 3.0$ MHz) also appears to be lost, although this feature is

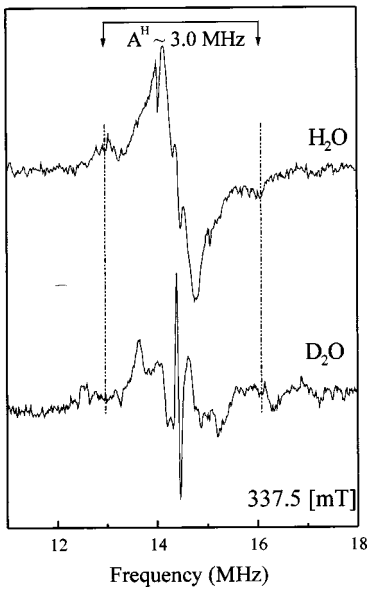

Figure 5 X-band ENDOR spectra (11–18 MHz) of the Mo(V) High-*g* [resting] signal, measured at 25 K: comparison of spectra before and after ^2H_2O exchange

The ENDOR field was 337.5 mT. Conditions: frequency, 9.47 GHz; microwave power, 5 mW; (nominal) radio frequency (RF) power, 100 W; RF modulation depth, 160 kHz.

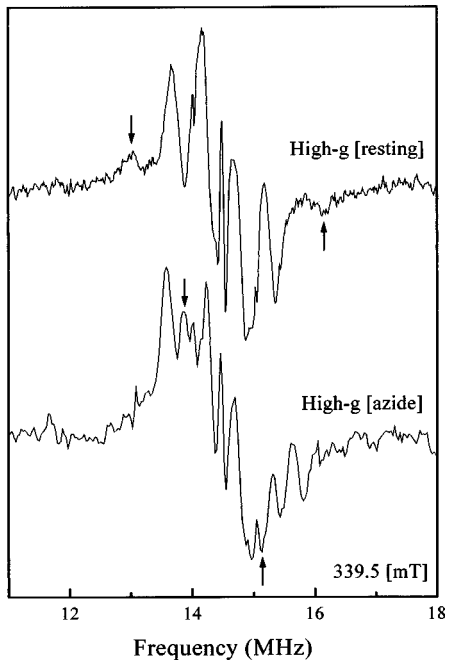

Figure 6 X-band ENDOR spectra (11–18 MHz) of Mo(V) High-*g* [resting] and High-*g* [azide] signals, measured at 25 K

The ENDOR field was 339.5 mT. Conditions: frequency, 9.47 GHz; microwave power, 5 mW; (nominal) radio frequency (RF) power, 100 W; RF modulation depth, 160 kHz.

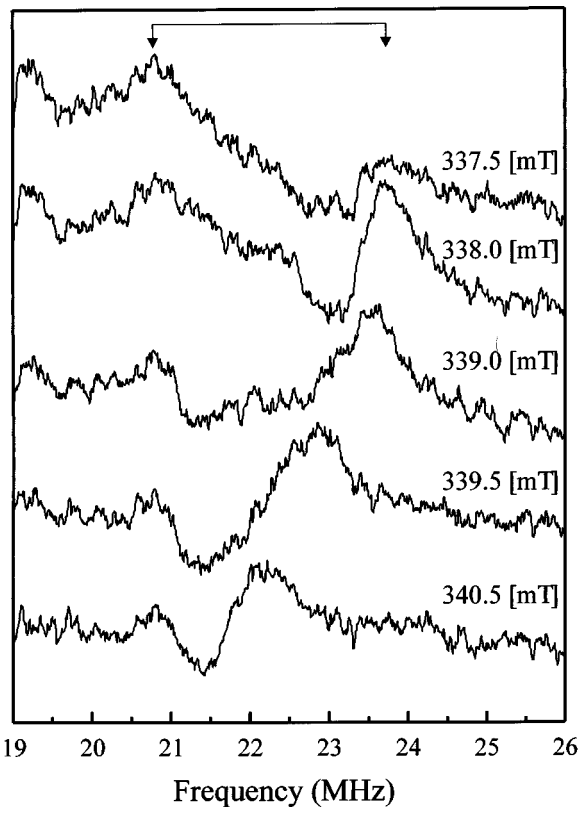

Figure 7 X-band ENDOR spectra (19–26 MHz) of the Mo(V) High-*g* [resting] signal, measured at 25 K, with baselines measured at off-EPR-resonance fields subtracted

ENDOR fields are indicated. The bar shows the extremes of movement of the features used in calculating the approximate Mo–H distance. Conditions: frequency, 9.41 GHz; microwave power, 5 mW; (nominal) radio frequency (RF) power, 100 W; RF modulation depth, 397 kHz.

less clearly resolved in the H_2O samples against the baseline noise. Additional unresolved exchangeable protons can be observed in Figures 4 and 5. The small A^H values of these weakly coupled proton clusters indicate molybdenum–proton distances in excess of 5 Å. Thus the solvent-exchangeable protons may arise from water molecules in the catalytic pocket, while the origin of the non-exchangeable protons may be the *bis*-MGD or catalytic pocket amino acid residues.

The effects of two potential Mo(V) ligands on the NAP_{Pp} ENDOR spectrum were also studied. The enzyme substrate, nitrate, had no discernible effect on the ENDOR spectrum, either after addition to the resting enzyme or after inclusion of dithionite to initiate turnover. This would be consistent with the view that nitrate binds to the Mo(IV) state of NAP rather than to the ENDOR-detectable Mo(V) state [16]. It has been demonstrated previously that a novel EPR signal can be generated by reducing NAP with dithionite in the presence of the competitive inhibitor azide, followed by oxidation to Mo(V) by ferricyanide. The spectrum (Figure 1), like the High-*g* [resting] signal, is split by weakly interacting $I = \frac{1}{2}$ nuclei ($A_{av} = 18.9$ MHz), which are also present in spectra collected from enzyme exchanged into ^2H_2O and are likely to arise from the β-carbon protons of the co-ordinating cysteine ligand (see below). ENDOR analysis of the High-*g* [azide] species reveals broad symmetrical resonance features, centred at $\nu_H = 14.5$ MHz, arising from coupled protons (Figure 6). Comparison with the High-*g* [resting] ENDOR spectrum shows that the solvent-exchangeable coupled proton with $A^H \sim 3.0$ MHz is lost at all orientations (results not shown), and other weakly coupled protons are detected. This suggests that binding of azide to Mo(IV) may displace an OH or H_2O species from the catalytic pocket.

Detailed analysis of the NAP_{Pp} (H_2O) spectra in the region of 22–24 MHz revealed weak features that are likely to arise from a strongly coupled proton (Figure 7). The low-frequency partner of such a species is expected at approx. 6 MHz, but was too weak to be detected. A pair of features at ~ 6 MHz and 22–24 MHz would have a coupling constant of $A^H \sim 18$ MHz, and so would be predicted from the major splitting ($A_1 \sim 17.83$ MHz) seen in the High-*g* [resting] EPR spectrum. The total anisotropy of this feature observed in the ENDOR spectra, measured at a number of fields across the EPR spectrum representing a number of different orientations of the molybdenum centre, was 3.5 MHz. This indicates a Mo–proton distance of approx. 3.2 Å (see the Experimental section), assuming that all the unpaired spin density is centred on Mo. Clearly this assumption is not true, but to obtain a more accurate value would require knowledge of the bonding geometry and spin densities at intermediate atoms. These weak features at 22–24 MHz from the strongly coupled proton were still detectable in deuterated buffer and in nitrate- and azide-treated samples (results not shown). Since a sulphur from a cysteine residue can be assumed directly to co-ordinate the Mo, it is reasonable to assign the weakly anisotropic non-exchangeable proton splittings observed in the EPR spectrum to the two β-carbon protons of the cysteine methylene group. The large value for the isotropic components of the couplings is also more consistent with delocalization via a cysteine sulphur, rather than a serine oxygen. Large isotropic couplings for cysteine sulphur bound to copper [23] or Fe [25] have been rationalized by considering that the metal–sulphur bonding orbital has π-

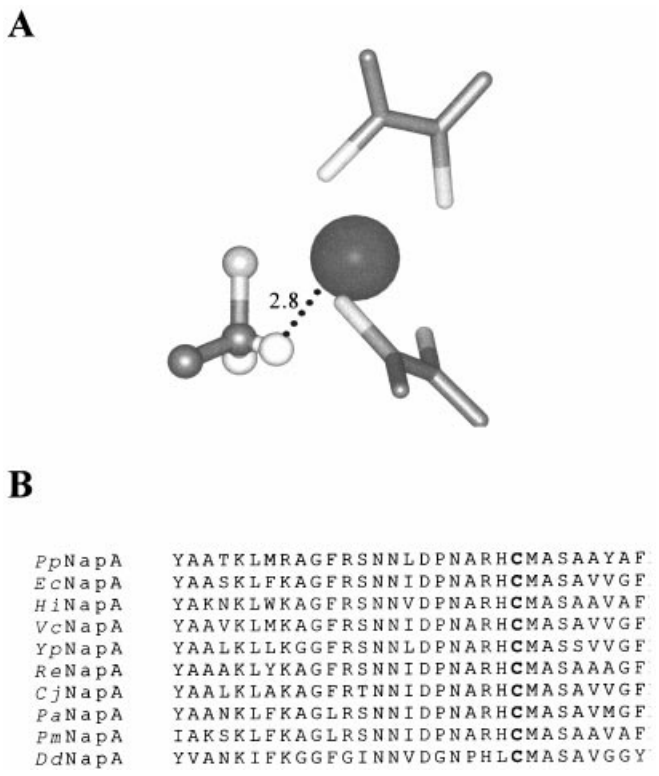

Figure 8 (A) Three-dimensional image of the Mo centre of NAP_{Dd} showing the co-ordinating cysteine ligand and the position of β-C methylene protons, and (B) multiple sequence alignment of a segment of NAP that provides the Mo–Cys ligand

Sequences are from: *Pp, Paracoccus pantotrophus; Ec, Escherichia coli; Hi, Haemophilus influenzae; Vc, Vibrio cholerae; Yp, Yersina pestis; Re, Ralstonia eutropha; Cj, Campylobacter jejuni; Pa, Pseudomonas aeruginosa; Pm, Pasteurella multocida; Dd, Desulfovibrio desulfuricans.*

symmetry, and that, at certain values of the H–C–S–metal dihedral angle, the C–H bond is orientated such that it is collinear with one of the lobes of this orbital. It is not possible to obtain useful estimates of this angle without knowing the spin density on the sulphur, which we are unable to estimate from our data, except to note that the very high value indicates a large overlap. Overall, the likely candidate for the strongly coupled proton at 22–24 MHz is one of the methylene protons of a cysteine ligand. This assignment would be consistent with the recently described crystal structure of NAP from *D. desulfuricans* [9] and site-specific mutagenesis studies on NAP_{Pp} (H. J. Sears, unpublished work). The crystal structure places the methylene carbon of Cys^{140} at a distance of 3.2 Å from the Mo, and the β-methylene protons at distances of 2.8 Å and 3.6 Å, using the HGEN programme of the CCP4 suite of programs (Figure 8). The crystallographically determined structure is for the oxidized NAP_{Dd}, and gives distances from the Mo to the dithiolene sulphurs of between 2.2 and 2.4 Å, and to the cysteine sulphur of 2.6 Å. However, although EXAFS measurements on a variety of oxidation levels of the NAP_{Pp} [16] indicate that most sulphurs remain at approx. 2.4 Å from the Mo, they also suggest that the distance between Mo and the cysteine sulphur can vary under different conditions; this implies that there is flexibility in the length of this bond, and therefore in the Mo–H distances. The proton splitting ($A_1^2 \sim 7.85$ MHz) resolved only in the g_x region of the EPR spectrum may arise from the second of the two cysteine methylene protons, but is not clearly resolved in the ENDOR spectra, where it would be expected to give rise to resonance features at approx. 11 MHz and 19 MHz.

EXAFS analysis of NAP_{Pp} has shown that it can be reduced from a Mo(VI) di-oxo species to a Mo(IV) mono-oxo species, and can be re-oxidized by nitrate back to a Mo(VI) di-oxo species [16]. During the reductive half-cycle of the reaction, Mo(VI) is two-electron-reduced to Mo(IV), with the concomitant protonation ($2H^+$) of one of the Mo–oxo ligands. This results in the release of a water molecule, leaving a vacant co-ordination site for nitrate binding. The question as to when the oxo group is protonated and removed as water is of interest to the catalytic cycle and will be relevant to determining the structure of the Mo(V) intermediate. We have suggested previously that it is the reduction of Mo(V) to Mo(IV) that is accompanied by the protonation of the oxo group to form water, since no evidence for a Mo(V)–OH or Mo(V)–OH_2 ligand can be readily detected in the EPR spectrum [16]. However, this assertion must be treated with caution, since it has been argued that protons of a bound hydroxy group in the high-pH forms of sulphite oxidase and NAR are difficult to detect by EPR because of anisotropic magnetic coupling and non-collinearity of $\boldsymbol{g}$ and $\boldsymbol{A}$ [26]. ENDOR is a much more sensitive probe of proton coupling, and has been used in the present study to confirm that the non-exchangeable, weakly coupled protons resolved in EPR spectra of NAP_{Pp} are likely to arise from the β-methylene protons of the Mo–Cys ligand. Although ENDOR detected two coupled protons ($A^H \sim 3.0$ and ~ 1.0 MHz) that are lost upon exchange into ^2H_2O buffer, and in one case displaced by azide, these are both too weakly coupled to arise from a Mo–OH or Mo–OH_2 ligand, and probably represent water molecules in the catalytic pocket. Thus the ENDOR data provide confirmation that there is no Mo(V)–OH/OH_2 ligand, and sustain the view forwarded previously [16] that protonation of one of the Mo(VI) oxygen ligands accompanies the reduction of Mo(V) to Mo(IV), rather than Mo(VI) to Mo(V). Thus, in the absence of an X-ray crystal structure for NAP_{Pp}, a combination of solution studies using EXAFS, EPR and ENDOR has indicated that the Mo co-ordination during the reductive half of the catalytic cycle may proceed from a di-oxo Mo(VI) to a mono-oxo Mo(IV) species without the involvement of a hydroxylated or hydrated Mo(V) intermediate. This would be distinct from the mono-oxo/des-oxo cycle proposed for NAP_{Dd} that proceeds via a Mo(V)–$OH_{(2)}$ intermediate [8]. The precise nature of the Mo(V) High-*g* species still cannot be determined unambiguously. It may have a vacant co-ordination site, although previous observations that the EPR signal was completely unperturbed by high concentrations of potentially strong exogenous ligands, including the enzyme substrate nitrate, could argue against this [16]. We have have also suggested previously that Mo(V) may be co-ordinated by an oxy group (-O) that may be stabilized by electrostatic interactions with a conserved positively charged arginine residue (Arg^{354}; NAP_{Pp} numbering) that has been implicated from the crystal structure [9] to anchor the bound substrate. The catalytic model for NAP_{Pp} based upon the EXAFS, EPR and ENDOR data would clearly be different from that derived from the crystal structure of NAP_{Dd}. This is rather surprising, given that NAP_{Pp} and NAP_{Dd} exhibit similar EPR spectra [16]. However, our sequence analysis of NAP_{Dd} reveals that it is the most divergent NAP reported to date, and this is particularly notable in the region of the polypeptide that provides the Mo–Cys ligand (Figure 8). NAP_{Pp} and NAP_{Dd} are the only members of the NAP family for which any significant biochemical and spectroscopic characterization is available. It would now be instructive to study the spectroscopic

properties of other members of the NAP family in more detail, in order to determine whether the differences in Mo co-ordination that we report arise from the divergence of the NAP_{Pp} and NAP_{Dd} primary structures.

We are grateful to David Clarke, Jeremy Thornton and Ann Reilly for help with the growth of *P. pantotrophus* and the purification of NAP. We also thank Dr Reinhard Kappl for helpful discussions. The work was supported by BBSRC grants CO8666 to D.J.R., B.C.B., A.J.T. and S.J.F., and BO3032-1 to the Centre for Metalloprotein Spectroscopy and Biology, University of East Anglia. D.J.L. and S.A.F. were supported by the BBSRC core strategic grant to the John Innes Centre.

REFERENCES

1 Sears, H. J., Little, P. J., Richardson, D. J., Spiro, S., Berks, B. C. and Ferguson, S. J. (1997) Identification of an assimilatory nitrate reductase in mutants of Paracoccus denitrificans GB17 deficient in nitrate respiration. Arch. Microbiol. **167**, 61–66

2 Berks, B. C., Ferguson, S. J., Moir, J. W. B. and Richardson, D. J. (1995) Enzymes and associated electron transport systems that catalyse the respiratory reduction of nitrogen oxides and oxyanions. Biochim. Biophys. Acta **1232**, 97–173

3 Ludwig, W., Mittenhuber, G. and Freidrich, C. G. (1993) Transfer of *Thiosphaera pantotropha* to *Paracoccus denitrificans*. Int. J. Syst. Bacteriol. **43**, 363–367

4 Berks, B. C., Richardson, D. J., Reilly, A., Willis, A. C. and Ferguson, S. J. (1995) The *napEDABC* gene cluster encoding the periplasmic nitrate reductase system of *Thiosphaera pantotropha*. Biochem. J. **309**, 983–992

5 Berks, B. C., Richardson, D. J., Robinson, C., Reilly, A., Aplin, R. T. and Ferguson, S. J. (1994) Purification and characterization of the periplasmic nitrate reductase from *Thiosphaera pantotropha*. Eur. J. Biochem. **220**, 117–124

6 Breton, J., Berks, B. C., Reilly, A., Thomson, A. J., Ferguson, S. J. and Richardson, D. J. (1994) Characterization of the paramagnetic iron-containing redox centers of *Thiosphaera pantotropha* periplasmic nitrate reductase. FEBS Lett. **345**, 76–80

7 Butler, C. S., Ferguson, S. J., Berks, B. C., Thomson, A. J., Cheesman, M. R. and Richardson, D. J. (2001) Assignment of heme ligands and detection of electronic absorption bands of molybdenum in the di-heme periplasmic nitrate reductase of *Paracoccus pantotrophus*. FEBS Lett. **500**, 71–74

8 Richardson, D. J., Sears, H. J., Spiro, S., Berks, B. and Ferguson, S. J. (1997) The bacterial nitrate reductases. In Advances en el Metabolismo del Nitrogeno: de la Fistologia a la Biologia Molecular (Vega, J. M., Pedro, J. A., Castillo, F. and Maldonado, J. M., eds.), pp. 565–574, Secretariado de Publicaciones de la Universidad de Sevilla, Porvenir, Sevilla

9 Dias, J. M., Than, M. E., Humm, A., Huber, R., Bourenkov, G. P., Bartunik, H. D., Bursakov, S., Calvete, J., Caldeira, J., Carneiro, C. et al. (1999) Crystal structure of the first dissimilatory nitrate reductase at 1.9 angstrom solved by MAD methods. Structure **7**, 65–79

10 Schindelin, H., Kisker, C., Hilton, J., Rajagopalan, K. V. and Rees, D. C. (1996) Crystal structure of DMSO reductase: Redox-linked changes in molybdopterin coordination. Science **272**, 1615–1621

11 Schneider, F., Löwe, J., Huber, R., Schindelin, H., Kisker, C. and Knäblein, J. (1996) Crystal structure of dimethyl sulfoxide reductase from *Rhodobacter capsulatus* at 1.88 angstrom resolution. J. Mol. Biol. **263**, 53–69

Received 2 August 2001/20 December 2001; accepted 12 February 2002

12 McAlpine, A. S., McEwan, A. G., Shaw, A. L. and Bailey, S. (1997) Molybdenum active centre of DMSO reductase from *Rhodobacter capsulatus*: crystal structure of the oxidised enzyme at 1.82-angstrom resolution and the dithionite-reduced enzyme at 2.8-angstrom resolution. J. Biol. Inorg. Chem. **2**, 690–701

13 Boyington, J. C., Gladyshev, V. N., Khangulov, S. V., Stadtman, T. C. and Sun, P. D. (1997) Crystal structure of formate dehydrogenase H: Catalysis involving Mo, molybdopterin, selenocysteine, and an Fe4S4 cluster. Science **275**, 1305b–1308

14 Czjzek, M., Dos Santos, J. P., Pommier, J., Giordano, G., Méjean, V. and Haser, R. (1998) Crystal structure of oxidized trimethylamine N-oxide reductase from *Shewanella massilia* at 2.5 angstrom resolution. J. Mol. Biol. **284**, 435–447

15 Bennett, B., Benson, N., McEwan, A. G. and Bray, R. C. (1994) Multiple states of the molybdenum center of dimethylsulfoxide reductase from *Rhodobacter capsulatus* revealed by epr spectroscopy. Eur. J. Biochem. **225**, 321–331

16 Butler, C. S., Charnock, J. M., Bennett, B., Sears, H., Reilly, A. J., Ferguson, S. J., Garner, C. D., Lowe, D. J., Thomson, A. J., Berks, B. C. and Richardson, D. J. (1999) Models for molybdenum coordination during the catalytic cycle of periplasmic nitrate reductase from *Paracoccus denitrificans* derived from EPR and EXAFS spectroscopy. Biochemistry **38**, 9000–9012

17 Butler, C. S., Charnock, J. M., Garner, C. D., Thomson, A. J., Ferguson, S. J., Berks, B. C. and Richardson, D. J. (2000) Thiocyanate binding to the molybdenum centre of the periplasmic nitrate reductase from *Paracoccus pantotrophus*. Biochem. J. **352**, 859–864

18 Howes, B. D., Bray, R. C., Richards, R. L., Turner, N. A., Bennett, B. and Lowe, D. J. (1996) Evidence favoring molybdenum-carbon bond formation in xanthine oxidase action. Biochemistry **35**, 1432–1443

19 Manikandan, P., Choi, E.-Y., Hille, R. and Hoffman, B. M. (2001) 35 GHz ENDOR characterisation of the ''Very Rapid'' signal of xanthine oxidase reacted with 2-hydroxy-6-methylpurine (^{13}C8): evidence against direct Mo-C8 interaction. J. Am. Chem. Soc. **123**, 2658–2663

20 Bennett, B., Berks, B. C., Ferguson, S. J., Thomson, A. J. and Richardson, D. J. (1994) Mo(V) electron-paramagnetic-resonance signals from the periplasmic nitrate reductase of *Thiosphaera-pantotropha*. Eur. J. Biochem. **226**, 789–798

21 Bray, R. C., Lowe, D. J., Capeillere-Blandin, C. and Fielden, E. M. (1973) Trapping of short lived intermediates in enzymic reactions by rapid-freezing: combination of electron paramagnetic resonance with pulse radiolysis. Biochem. Soc. Trans. **1**, 1067–1072

22 Atherton, N. M. (1973) Electron Spin Resonance, Wiley, New York

23 Neese, F., Kappl, R., Hüttermann, J., Zumft, W. and Kroneck, P. M. H. (1998) Probing the ground state of the purple mixed valence Cu_A centre in nitrous oxide reductase: a CW ENDOR (X-band) study of the ^{65}Cu, ^{15}N-histidine labeled enzyme and interpretation of hyperfine couplings by molecular orbital calculations. J. Biol. Inorg. Chem. **3**, 53–67

24 Sears, H. J., Bennett, B., Spiro, S., Thomson, A. J. and Richardson, D. J. (1995) Identification of periplasmic nitrate reductase Mo(V) signals in intact cells of *Paracoccus denitrificans*. Biochem. J. **310**, 311–314

25 Kappl, R., Ciurli, S., Luchinat, C. and Hüttermann, J. (1999) Probing structural and electronic properties of the oxidized $[Fe_4S_4]^{3+}$ cluster of *Ectothiorhodospira halophila* iso-II high potential iron-sulfur protein by ENDOR spectroscopy. J. Am. Chem. Soc. **121**, 1925–1935

26 George, G. N. (1985) The proton spin-flip lines of Mo(V) electron-paramagnetic-resonance signals from sulfite oxidase and xanthine-oxidase. J. Magn. Reson. **64**, 384–394